Feedback design for 3D movement of an Eel-like robot

M. Alamir, M. El Rafei, G. Hafidi, N. Marchand, M. Porez and F. Boyer

***Abstract*— This paper relates recent advances in the design of feedback laws for the 3D movement of an Eel-like robot. Such a robot is under construction in the context of a national French robotic project. The proposed feedback enables the tracking of a desired 3D position of the Eel head as well as the stabilization of the rolling angle. A velocity controller is also proposed. The controller is tested on a recently developed complete 3D model in order to assess its efficiency in tackling 3D manoeuvres.**

I. INTRODUCTION

This paper presents current researches on the control of an eel-like robot. This is done in the context of a multi-disciplinary French national research project called ROBEA-ANGUILLE[1]. The aim of this project is to design, construct and control the 3D motion of an eel-like robot. The prototype under construction is obtained by connecting many parallel platforms. The eel's body will then be covered by a deformable "*skin*" in order to achieve high performances swimming. As it has been underlined by many researchers in the robotic biomimetic field, understanding the dynamics of such robots may be of a great interest in improving the manoeuvrability of under-water vehicles [18], [9], [12], [10], [6], [14], [17], [1].

A 3D continuous model of the target prototype has been recently proposed in [2] using the geometrically exact theory of beams in finite deformations [15]. This model is used here to validate the proposed $3D$ control feedback.

The main works more in the spirit of this paper are due to [10] (and the related works) where the 2D movement of an eel-like robot has been studied. The rolling cart analogy is used in order to derive state feedback that track some reference trajectories. Another interesting approach was proposed in [11], [12], [19] where averaging formulas have been derived to describe the mean behavior over a cycle. Recent work has been developed in [8] where a control design based on Lyapunov methods was used for planning motion. A design procedure for a biomimetic robot-fish based on improved kinematic propulsive model has been described in [20] where the basic motion control laws were presented. For a detailed review of existing works on control of swimming, the reader can refer to [6].

This work was support by the French National Center for Scientific Research (CNRS) in the context of the ROBEA-project.

M. Alamir, M. El Rafei, N. Marchand and G. Hafidi are with the Automatic control department of GIPSA-Lab mazen.alamir@inpg.fr, nicolas.marchand@inpg.fr, ghizlane.hafidi@supelec.fr , maher.el-rafei@lag.ensieg.inpg.fr

M. Porez and F. Boyer are with the Institut de Recherche en Cybernétique de Nantes. frederic.boyer@emn.fr, mathieu.porez@irccyn.ec-nantes.fr

[1]http://www.irccyn.ec-nantes.fr/hebergement/ROBEA/

However, few researches has studied the control methods for 3D motion of fish robots. In our work, a complete control scheme for 3D movement of the robot's continuous model [2] is proposed. Basically, the motion and the velocity in the transverse plane are controlled by monitoring the oscillatory gait characteristics while the altitude changes and the rolling stabilization task are handled by means of two pectoral fins that are attached to the eel's head (see figure 2) (practical applications of pectoral fins are more detailed in [7], [1]). Our basic concern while developing the control strategy was the simplicity and the robustness against modeling errors. To achieve this, very simple feedback laws have been derived that are quite independent of the structure of the simulator equations. The latter is only used to assess the performance of the proposed feedback laws. In other words, since the controller uses too few information about the simulation model, it is likely to work on the real system (probably after some tuning phase) even if it differs from the simulation model used here to assess its performance.

This paper is organized as follows : First, the mathematical model used in the simulator is briefly described in section II. Since the latter is quite complex, only the related guidelines are briefly mentioned. Section III clearly states the $3D$ control problem. The different "*components*" of the feedback law are then presented in section IV, namely, the control of the head position in the transverse plane, the control of the robot altitude as well as the rolling angle stabilization. The control of the robot mean velocity is discussed in section V before some $3D$ scenarios are proposed in section VI. The paper ends by some concluding remarks together with the road map for future works.

II. THE MATHEMATICAL MODEL OF THE CONTINUOUS EEL-LIKE ROBOT

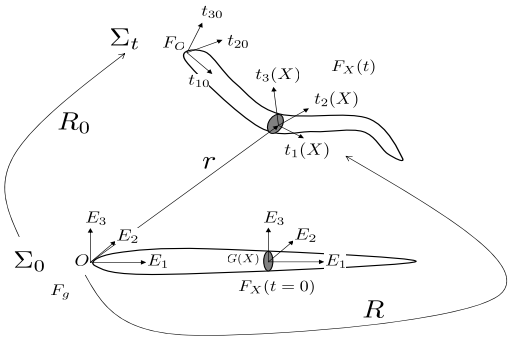

Fig. 1. Frames and parametrization of the continuous eel robot model

For a complete description of the underlying mathematical

model, the reader is referred to the basic paper [2]. Only the main features of the model in the non stretchable case are mentioned here in order to give an idea about the model complexity and how the $3D$ features are handled.

Figure 1 illustrates the basic notations used in the description of the mathematical model. Let X designates the material abscissa along the eel's mean line and $G(X)$ the center mass of X section. Under the assumption of non-stretchable body, the configuration of the robot at instant t (after deformation) is completely defined by the value at each $X \in [0,1]$ of the rotation matrix $R(t,X)$ mapping the X mobile basis before deformation on to after (see figure 1).

Once given the rotation matrix and the position of the head , namely $R_0(t) = R(t,0)$ and $r_0(t) = r(t,0)$, the deformation of the body is completely defined by $\frac{\partial R}{\partial X}$ that can be written as follows :

$$\frac{\partial R}{\partial X} = R\hat{K} \quad ; \quad R(t,0) = R_0, \tag{1}$$

where $\hat{K}(t,X)$ is a skew symmetric tensor associated to an axial vector $K(t,X)$. Note that (1) is nothing but a change in the description variables since $\hat{K} = R^T \frac{\partial R}{\partial X}$ becomes the new d.o.f that defines the deformation of the eel's body. Note that the last two components of K, namely K_2 and K_3 stand for the curvatures of the beam in the two planes $(G, t_1, t_3)(t,X)$ and $(G, t_1, t_2)(t,X)$ while the first component K_1 stands for the torsion strain field.

It is important to note immediately that in the present paper, the vector field $K(\cdot,\cdot)$ is a part of the control input (together with the angles of the pectoral fins described later in the paper). This assumes that the distributed actuators are conveniently used to produce the corresponding body deformation in within the allowable powers and excursions. The choice of the controller/setpoints parameters that makes this possible is not explicitly discussed in the present paper. One may easily imagine how this can be made by a kind of performance tuning approach.

Using the above notations, the non stretching assumption can be expressed as follows :

$$r' := \frac{\partial r}{\partial X} = t_1(t,X) \quad ; \quad r(t,0) = r_0(t). \tag{2}$$

Let us now introduce the field of angular velocities $\hat{\omega}(t,X)$:

$$\hat{\omega} = \dot{R}R^T \quad \text{(that is } \dot{R} = \hat{\omega}R\text{)}. \tag{3}$$

The field $\hat{\omega}$ can also be represented by its axial vector ω. It can be proved (see [4]) that :

$$\frac{\partial \omega}{\partial X} = R\dot{K} \quad ; \quad \omega(t,0) = \omega_0(t). \tag{4}$$

This means that, given the control $K(\cdot,\cdot)$ and the configuration $R(\cdot,\cdot)$, the integration of (4) in space enables the computation of ω, hence $\hat{\omega}$ and therefore $\dot{R}$ thanks to (3).

On the other hand, by differentiating (2) in time, it comes that :

$$\frac{\partial \dot{r}}{\partial X} = \omega \times t_1 \quad ; \quad \dot{r}(t,0) = \dot{r}_0(t),$$

that can be integrated in order to reconstruct $\dot{r}(t,X)$ for all $X \in [0,1]$. Similarly, further derivations enables to write the second derivatives $\ddot{r}$ and $\dot{\omega}$ as functions of the head accelerations $\ddot{r}_0$ and $\dot{\omega}_0$, the velocities $\dot{r}_0$, ω_0 and the time derivatives of the strains field K. This can be shortly written as follows :

$$\begin{pmatrix} \ddot{r} \\ \dot{\omega} \end{pmatrix}(t,X) = \Gamma\Big(t, X, K(\cdot,\cdot), \dot{r}_0, \omega_0, \ddot{r}_0, \dot{\omega}_0\Big). \tag{5}$$

Note that the map Γ uses the control profile $K(\cdot,\cdot)$ in time and space through time derivations and integration over space as it has been done above for the computation of the velocities $\dot{r}$ and ω. Note that (5) expresses only kinematic constraints. In order to built the dynamic model, the external forces due to the contact with the fluid have to be computed. Assuming that the gravity forces are compensated by internal "*air tanks*", the only external forces are those due to the interaction of the body and the pectoral fins with the fluid. To express these forces and torques, the contact model of [13], [3] is used. This amounts to integrate the following quantities along the eel's body :

$$\frac{df_{ext}}{dX} = -\sum_{i=1}^{3} C_{1i}[|V_i|V_i]t_i - \sum_{i=1}^{3}[C_{2i}\gamma_i]t_i, \tag{6}$$

$$\frac{dc_{ext}}{dX} = -\sum_{i=1}^{3} C_{3i}[|\Omega_i|\Omega_i]t_i - \sum_{i=1}^{3}[C_{4i}\Xi_i]t_i, \tag{7}$$

where V_i, γ_i, Ω_i and Ξ_i are the components on t_i of $\dot{r}$, $\ddot{r}$, ω_i and $\dot{\omega}_i$ respectively, namely :

$$\dot{r} =: \sum_{i=1}^{3} V_i t_i \ ; \ \ddot{r} =: \sum_{i=1}^{3} \gamma_i t_i \ ; \ \omega =: \sum_{i=1}^{3} \Omega_i t_i \ ; \ \dot{\omega} =: \sum_{i=1}^{3} \Xi_i t_i$$

while $\{C_{ji}\}$ are coefficients depending on the mass per unit volume of the fluid, the shape and the size of the section (elliptic in our case) and the Reynolds number of the moving section in the fluid. Note that the first term of (6) accounts for the drag/lift forces applied on the section while the second term accounts for the added mass forces as given by [16]. The same angular related significations hold for the terms in (7). Note that the external forces and torques obtained

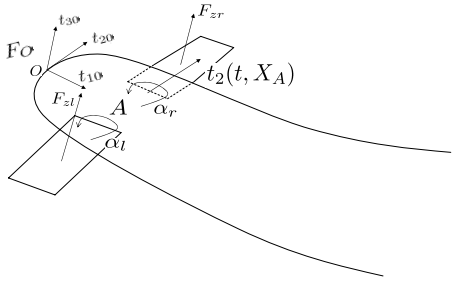

Fig. 2. Pectoral fins positions and the induced forces

from the spacial integration of (6)-(7) are those generated by the contact forces along the Eel's body. The expressions of the external forces and torques due to the pectoral fins

are to be added. These forces and torques can be obtained using the same kind of formulations as (6)-(7) that have to be integrated along the pectoral fins surfaces (see figure 2). The fins are attached at some point A on the Eel's head. Their axis of rotation coïncide with $t_2(t, X_A)$. The corresponding angles are denoted by α_r and α_l respectively. More precisely, α_r [resp. α_l] vanishes when the right [resp. left] fin lies in the plane $(A, t_1(t, X_A), t_2(t, X_A))$. Writing the corresponding expressions similar to (6)-(7) gives the fin's related distribution of forces and torques denoted hereafter by :

$$\frac{\partial f_a^j}{\partial s} \quad ; \quad \frac{\partial c_a^j}{\partial s} \quad ; \quad j \in \{r, l\}$$

where s is the curvilinear abscissa along the axis of the fin, namely $t_2(t, X_A)$ while $\frac{\partial f_a^j}{\partial s} ds$ and $\frac{\partial c_a^j}{\partial s} ds$ are the infinitesimal forces and torques applied on a slice of width ds perpendicular to this axis.

III. STATEMENT OF THE CONTROL PROBLEM

First of all, in accordance with the behavior of true eels, only the component K_3 of the deformation field is used. Namely, at any time t, the body mean line entirely lies in the plane $(0, t_{10}(t), t_{20}(t))$:

$$K_1 \equiv 0 \quad ; \quad K_2 \equiv 0.$$

The control problem is schematically depicted on figure 3. A target position P_d is given that is not necessarily in the transverse plane $(0, t_{10}, t_{20})$ of the eel's mean line. The controller has to appropriately modify the control input :

$$\mathbf{u} := \begin{pmatrix} K(\cdot,\cdot) & \alpha_r & \alpha_l \end{pmatrix}; \quad (\alpha_r, \alpha_l) \in [-\alpha_{max}, +\alpha_{max}]^2$$

in order to steer the head O towards the desired position P_d. Note however that we are not interested in point-wise

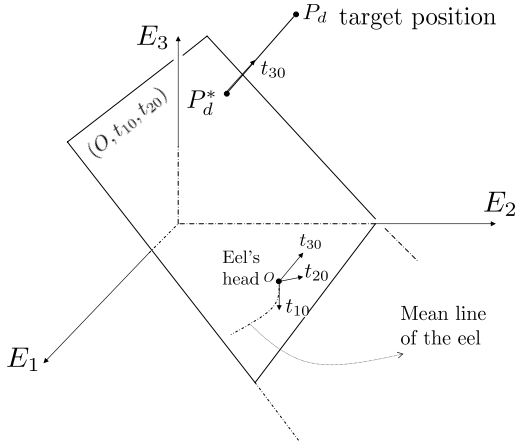

Fig. 3. Schematic 3D view of the control problem. The Eel that lies at instant t in the plane $(0, t_{10}(t), t_{20}(t))$ has to join the target position P_d while trying to keep the vector t_{20} horizontal, namely $t_{20} \cdot E_3 \approx 0$. This has to be done using the infinite dimensional control input $(K(\cdot,\cdot), \alpha_r, \alpha_l)$.

stabilization at P_d since the effectively used P_d will be later generated by tl-operation mode[2] and will be continuously moving. This is because the eel robot falls in the class of systems (including the rolling cart, the snakeboard, etc.) that cannot be controlled at zero-velocity. In addition to the control objective consisting in steering the eel's head to the desired position P_d, the rolling angle of the body has to be controlled. When the eel is in arbitrary $3D$ configuration, expressing the desired rolling angle is not an easy task. Many choices can be done. Here, the controller is oriented towards the regulation of the scalar product :

$$p_{rol} := t_{20} \cdot E_3$$

around 0. Indeed, this guarantees that when the eel mean line lies in a horizontal plane, its transverse plane is also horizontal. Moreover, we look for a feedback law enabling the mean velocity of the head, namely $V_0 = \frac{1}{T} \int_{t-T}^{t} \|\dot{r}_0(\tau)\| d\tau$ to be controlled by appropriately controlling the characteristic of the body deformation through the control input $K(\cdot,\cdot)$.

IV. THE PROPOSED FEEDBACK

Recall that $K_1 \equiv K_2 \equiv 0$. The undulation law K_3 takes the following form in accordance with biological observations [5] :

$$K_3(t, X) := u_3 \cdot A(X, u_2) \sin(\frac{X}{\lambda} - \frac{t}{T}) + u_1, \qquad (8)$$

where $u_3 \cdot A(X, u_2)$ gives the amplitude of the undulation as a function of the material abscissa X. The control input $u_3 \in [0, u_3^{max}]$ scales the amplitude in order to control the velocity as explained later on. On the other hand, the control input $u_2 \in \{-1, 1\}$ defines whether the amplitude of undulations is bigger at the eel's tail or the eel's head. This is used to enhance acceleration or deceleration according to the velocity related control requirements.

The remaining control input $u_1 \in [-u_1^{max}, u_1^{max}]$ is used to control the eel's movement in the transverse plane as it is explained in the following section.

A. Controlling the movement in the transverse plane $(0, t_{10}, t_{20})$

The way this is done is based on the following observation : When the undulation law (8) is used with $u_1 \equiv 0$, a straight movement in the plane $(0, t_{10}, t_{20})$ is asymptotically obtained while constant non vanishing values of u_1 lead to circular trajectories.

Therefore, the control law uses u_1 to correct the direction of the movement in the plane $(0, t_{10}, t_{20})$ in order to "*move strait towards*" the target position P_d^*. Note that P_d^* is the projection *parallel to* t_{30} of P_d on the plane $(0, t_{10}, t_{20})$ (see figure 3). The feedback uses the following key quantities :

$$p_{ext} := -\pi_3\big(\overrightarrow{OP_d^*} \wedge t_{10}\big) \quad ; \quad p_{sc} = -\overrightarrow{OP_d^*} \cdot t_{10}$$

where $\pi_3(\cdot)$ designates the third component of the argument. With the above notations, the following feedback is defined on u_1 :

$$\begin{aligned} u_1(t) &= F_1(\overrightarrow{OP_d^*}(t), t_{10}(t)) \\ &:= \begin{cases} -\beta_c \cdot \bar{p}_{ext}(t) & \text{if } \bar{p}_{sc}(t) > 0 \\ u_1^{max} & \text{otherwise} \end{cases} . \end{aligned} \qquad (9)$$

[2]http://www.lag.ensieg.inpg.fr/alamir/

where $\bar{p}_{ext}(t)$ and $\bar{p}_{sc}(t)$ are the mean values of p_{ext} and p_{sc} over the past period of undulation, namely :

$$\bar{p}_{ext}(t) = \frac{1}{T}\int_{t-T}^{t} p_{ext}(\tau)d\tau \quad ; \quad \bar{p}_{sc}(t) = \frac{1}{T}\int_{t-T}^{t} p_{sc}(\tau)d\tau \quad (10)$$

This amounts to stabilize $\bar{p}_{ext}$ to 0 with $\bar{p}_{sc} > 0$ which means by definition of p_{ext} and p_{sc} that $-t_{10}$ and $\overrightarrow{OP_d^*}$ are parallel (in average) and in the same direction. Once this is reached, u_1 vanishes and the eel adopts no mean curvature and moves towards the projected target P_d^* with a strait mean line. The conditional use of $u_1 = u_1^{max}$ enables a maximal curvature to be used when the eel moves in the opposite direction to the one that would be necessary to move towards P_d^* and since this corresponds to a circular trajectory, the sign of p_{sc} necessarily becomes > 0 after a finite time after which the above argumentation holds.

Note that during three dimensional manoeuvres, the transverse plane $(0, t_{10}, t_{20})$ moves. This makes the projected position P_d^* moving even for fixed target state P_d.

B. Controlling the altitude

While in the preceding section, a feedback is defined that forces the eel to move towards the projected target position P_d^* in the transverse plane $(0, t_{10}, t_{20})$. The aim of the present section is to show how the altitude of the head is controlled by monitoring the pectoral fins angles. This is done by controlling the following variable :

$$z := r_0(t) \cdot E_3 \quad (11)$$

around the desired value $z_d := \pi_3(P_d)$. In order to achieve this task, it is worth noting that the dynamics of z is governed by the following equation :

$$\ddot{z}(t) = F_3(\alpha_r, \alpha_l, \dot{r}_0(t), \omega_0(t)) + \delta F \quad (12)$$

where $F_3(\cdot)$ is the component of the aerodynamic forces on E_3 while δF stands for effects on z of unknown forces (those generated by the whole body movement inducing acceleration at the head level).

The idea is then to design a robust sliding mode controller for which the switching surface is defined by :

$$S := \dot{z} + \lambda_3(z - z_d)$$

Time derivation together with (12) gives :

$$\dot{S} \quad = \quad F_3(\alpha_r, \alpha_l, \dot{r}_0(t), \omega_0(t)) + \delta F + \lambda_3 \dot{z}$$

Now, since the lift force is roughly determined by the sum of the fins angles $\alpha_s = \alpha_r + \alpha_l$, the last equation suggests to compute α_s according to :

$$\hat{\alpha}_s = arg \min_{\alpha_s \in [-2\alpha_{max}, +2\alpha_{max}]} J(\alpha_s, \dot{r}_0(t), \omega_0(t), z, \dot{z}) \quad (13)$$

where $J(\cdot)$ in (13) is given by :

$$J(\cdot) := \Big| F_3(\frac{\alpha_s}{2}, \frac{\alpha_s}{2}, \dot{r}_0(t), \omega_0(t)) + \lambda_3 \dot{z} - \mu_s Sign(S) \Big| \quad (14)$$

since when the optimal value of J vanishes and provided that $\mu_s > |\delta F|$, stability follows from :

$$\dot{S} < -(\mu_s - |\delta F|)Sign(S). \quad (15)$$

Note that for straightforward practical reasons, the Sign function is replaced by the following continuous function :

$$S_\varepsilon(\rho) := \begin{cases} \frac{\rho}{\varepsilon} & \text{if } |\rho| \leq \varepsilon \\ 1 & \text{if } \rho = \varepsilon \\ -1 & \text{if } \rho = -\varepsilon \end{cases} \quad (16)$$

Note that (13) gives the desired sum $\hat{\alpha}_r + \hat{\alpha}_l$. Later on, it is shown how the rolling angle control law gives a desired value of the difference $\hat{\alpha}_d = \hat{\alpha}_r - \hat{\alpha}_l$. The control input setpoints α_r and α_l are therefore given by :

$$\begin{pmatrix} \hat{\alpha}_r \\ \hat{\alpha}_l \end{pmatrix} = \begin{pmatrix} 1 & 1 \\ 1 & -1 \end{pmatrix}^{-1} \begin{pmatrix} \hat{\alpha}_s \\ \hat{\alpha}_d \end{pmatrix} \quad (17)$$

the way $\hat{\alpha}_d$ is computed in order to control the rolling angle is described in the following section.

C. Controlling the rolling angle

As it is indicated earlier, the control of the rolling angle amounts to control $p_{rol} := t_{20} \cdot E_3$ around 0. The evolution of p_{rol} follows basically the following law :

$$\ddot{p}_{rol} \sim k_{rol} \cdot (\alpha_r - \alpha_l) = k_{rol} \cdot \alpha_d.$$

where the difference α_d is supposed to belong to $[-\beta_{max}, +\beta_{max}]$. This suggests the following feedback law :

$$\begin{aligned} \hat{\alpha}_d \quad &:= \quad \beta_{max} \tanh\Big(-\kappa_1 p_{rol} - \kappa_2 \dot{p}_{rol}\Big) \\ &:= \quad \beta_{max} \tanh\Big(-\kappa_1 p_{rol} - \kappa_2 \pi_3(\omega_0 \times t_{20})\Big), \end{aligned} \quad (18)$$

where the use of the $tanh$ function enables the saturation on α_d to be satisfied. Recall that this is used in (17) together with (13) in order to completely determine the fins angles α_r and α_l.

V. Controlling the mean velocity

In this section, it is shown how the oscillatory gait characteristics can be monitored in order to control the mean velocity of the robot's head, namely :

$$V_0(t) = \frac{1}{T}\int_{t-T}^{t} \|\dot{r}_0(\tau)\| d\tau$$

More precisely, the degrees of freedom used here are u_2 and u_3 involved in the amplitude of the oscillation given by $u_3 A(X, u_2)$ in (8). In this section, the following definition is used for $A(X, u_2)$:

$$A(X, u_2) := \begin{cases} \sqrt{X} & \text{if } u_2 = +1 \\ \sqrt{1 - X} & \text{if } u_2 = -1 \end{cases} \quad (19)$$

First, the dynamic of the velocity is identified. For this, start-up scenarios have been simulated from rest by using different values of the pair $(u_2, u_3) \in \{-1, +1\} \times [0, u_3^{max}]$.

The obtained dynamic model is presented by the following form :

$$\dot{V}_0 = -(\beta_1 u_3 + \beta_2)\Big[V_0 - u_2 V_\infty(u_3)\Big]. \quad (20)$$

Namely, both the response time and the asymptotic values depend on u_3. The coefficients β_1, β_2 as well as the function $V_\infty(u_3)$ are obtained by identification. The identification

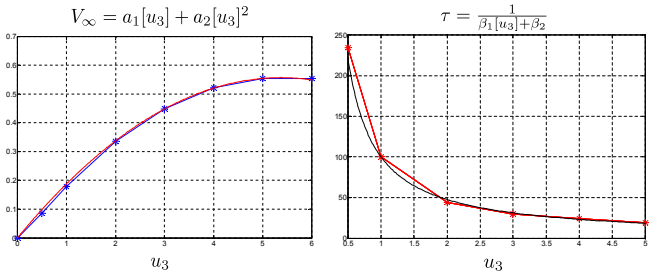

Fig. 4. Identification of the terms $V_\infty(u_3)$, β_1 and β_2 of the dynamic model (20) of the mean velocity V_0. Comparison between simulated and computed values.

results are shown on figures 4. Based on the identified model (20), monitoring u_2 and u_3 to control the mean velocity around some desired value V_0^d amounts to solve in the unknowns :

$$(\lambda_V, u_2, u_3) \in [0, \infty] \times \{-1, +1\} \times [0, +u_3^{max}]$$

the following nonlinear equation that simply states that the r.h.s of (20) is equal to $-\lambda_V(V_0 - V_0^d)$:

$$V_0 - u_2 V_\infty(u_3) = \frac{\lambda_V(V_0 - V_0^d)}{\beta_1 u_3 + \beta_2} \tag{21}$$

which is always possible provided that the desired velocity V_0^d is within the range of achievable velocities. Moreover, it can be shown that in this case, a simple and efficient golden section based search enables a solution to be found.

VI. Numerical simulations using the 3D continuous model [2]

In this section, some numerical simulations are proposed to assess the efficiency and underline some interesting features of the 3D movement control problem.

A. 3D manoeuvres without velocity control

In this section, simulations of a 3D manoeuvre with constant values for the control inputs u_2 and u_3 is proposed. Keeping these control inputs constant means that no feedback is done to control the mean velocity of the robot. This means that the robot cannot stop at the desired position. Once a neighborhood of the desired position is reached, the controlled robot can only "*turn around*" it waiting for the next set-point change. In what follows, some parameters used in the simulation are given.

B. The robot parameters

The exhaustive definition of the model parameters is given in [2]. Let us mentioned here that the length of the robot is $L = 2.08\ m$ and all the cross sections are ellipsoidal with evolutive dimension that reproduces a quite realistic and faithful form (the tail is thinner that the central body). The pectoral fins are positioned at $0.3\ m$ from the head.

C. Control related parameters

- The undulation period $T = 1.2\ s$ [see (8)]
- the wavelength $\lambda = 1.3\ m$
- The feedback gain $\beta_c = 1$ [see (9)]
- The saturation level $u_1^{max} = 0.5$ [see (9)]
- Sampling period $\tau_s = 0.1\ s$
- The z control parameters $(\lambda_3, \varepsilon, \mu_s) = (0.12, 0.05, 2.0)$ [see (13) and (16)]
- Saturations on the fins angles sum and difference $(\alpha_{max}, \beta_{max}) = (30\,\text{deg}, 20\,\text{deg})$ [see (13) and (18)]
- The rolling angle feedback gains $(\kappa_1, \kappa_2) = (4, 4)$ [see (18)]

D. Manoeuvre description

Three set-point changes are successively and simultaneously done on the three coordinates of the desired position P_d. The robot is initially at rest with the head at the origin "*oriented*" towards the negative values of x. The desired state is then defined by the following expression :

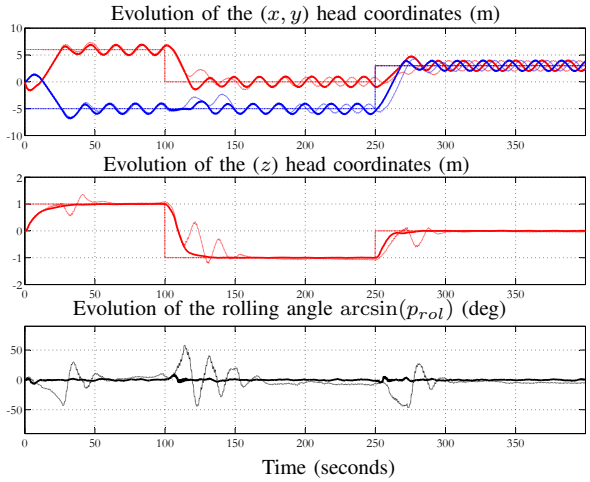

Fig. 5. Behavior of the controlled robot with (solid line) and without (dotted line) the rolling angle control under the three successive set-point changes given by (22).

$$P_d(t) = \begin{cases} (6, -5, 1)^T & \text{for } t \leq 100\ s \\ (0, -5, -1)^T & \text{for } 100 < t \leq 250\ s \\ (3, 3, 0)^T & \text{for } t > 250\ s \end{cases} \tag{22}$$

Figure 5 shows the behavior of the head's coordinates as well as the evolution of the rolling angle $\arcsin(p_{rol})$ when all the controllers are fired (solid line) and when the rolling angle controller is *switched off* (dotted thin line). This enables the coupling feature to be appreciated. Namely, when the rolling angle is badly controlled, effects on the altitude regulation can be observed. The evolution of the control variable $(\alpha_s, \alpha_d, u_1)$ during this scenario is depicted on figure 6. Note that except for the transient phases that follows set-point changes, the control input u_1 makes the robot "*turn around*" the desired position P_d since no velocity control is applied.

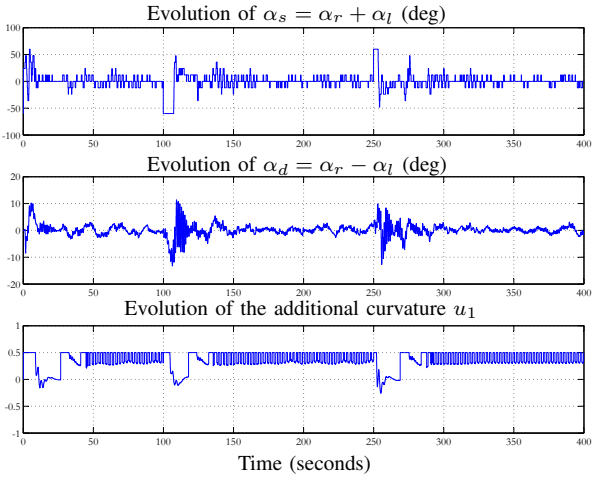

Fig. 6. Evolutions of the sum and difference of the pectoral fins angles (α_s, α_d) as well as the additional curvature u_1 during the scenario of figure 5.

E. Velocity control

In this section, the mean velocity controller developed in section V is tested. The parameters $(u_3^{max}, \lambda_V) = (5, 0.06)$ are used in (21). No controller are used on the other coordinates, namely $u_1 = \alpha_r = \alpha_l = 0$. The behavior of the closed loop system is depicted on figure 7 for different scenario, namely: a) Successive change in the constant desired velocity. b) A parabolic desired velocity and c) A ramp-like desired velocity.

It can be noticed that the quality of the regulation is better for increasing than for decreasing velocities. This is due to the fact that the identification of the model (20) is done using acceleration scenarios. Another reason is that the simulated Eel is not rigorously symmetric (the cross section smoothly varies from the head to the tail to reproduce the true eel's form).

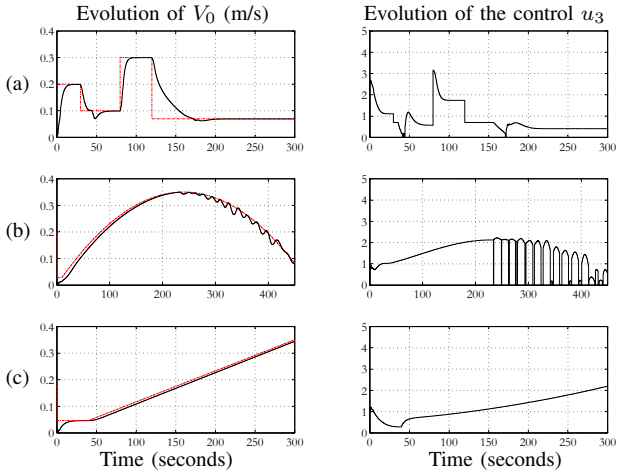

Fig. 7. Evolution of the mean velocity V_0 (m/s) under the control law of section V for three different profiles of the desired velocity.

VII. Conclusion

In this paper, preliminary results on the 3D control of an eel-like robot are presented. The proposed feedback is quite simple and independent of the detailed structure of the robot's model. The controller is validated using the complex continuous model of [2]. Future work concerns the implementation on the prototype (under construction). For this, a systematic identification and tuning strategy needs to be developed.

References

[1] P. R. Bandyopadhyay. Trends in biorobotic autonomous undersea vehicles. *IEEE Journal of Oceanic Engineering*, 30(1):109–139, January 2005.

[2] F. Boyer, M. Porez, and W. Khalil. Macro-continuous computed torque algorithm for a three-dimensional eel-like robot. *IEEE Transaction on Robotics and Automation*, 22(4):763–775, August 2006.

[3] J. J. Burgess. Bending stiffness in a simulation of undersea cable deployment. *Int. J. of Offshore and Polar Engineering*, 3(3), 1993.

[4] A. Cardona and M. Géradine. A beam finite element nonlinear theory with finite rotations. *Int. J. Numer. Meth. Engng*, 26:2403–2438, 1988.

[5] J. Carling, T. L. Williams, and G. Bowtell. Self-propelled anguilliform swimming: simultaneous solution of the two-dimensional navier-stokes equations and newtons laws of motion. *Journal of experimental biology*, 201:3143–3166, 1998.

[6] J. E. Colgate and K. M. Lynch. Mechanics and control of swimming: A review. *IEEE Journal of Oceanic Engineering*, 29(3):660–73, July 2004.

[7] N. Kato, H. Liu, and H. Morikawa. Biology-inspired precision maneuvering of underwater vehiclespart 3. *International Journal of Offshore and Polar Engineering*, 15(2):81– 87, June 2005.

[8] L. lapierre and B. Jouvencel. Path following control for an eel-like robot. *Oceans 2005 - Europe*, 1:460– 465, 2005.

[9] R. Mason and J. W. Burdick. Experiments in carangiform robotic fish locomotion. In *Proceedings of the IEEE Int. Conf. Robotics and Automation*, pages 428–435, San Francisco, 2000.

[10] K. A. McIsaac and J. P. Ostrowski. A geometric approach to anguiliform locomotion modelling of an underwater eel robot. In *Proceedings of the IEEE Int. Conf. Robotics and Automation*, pages 2843–2848, Detroit, 1999.

[11] K. A. Morgansen, V. Duidam, R. J. Mason, J. W. Burdick, and R.M. Murray. Nonlinear control methods for planar carangiform robot fish locomotion. volume 1, pages 427–434, 2001.

[12] K. A. Morgansen, P. A. Vela, and J. W. Burdick. Trajectory stabilization for a planar carangiform robot fish. In *Proceedings of the IEEE Int. Conf. Robotics and Automation*, pages 756–762, Washington, 2002.

[13] J. R. Morison. The force exerted by surface waves on piles. *Transactions of the AIME*, 189:149–154, 1950.

[14] M. Sfakiotakis, D. M. Lane, and B. C. Davies. Review of fish swimming modes for aquatic locomotion. *IEEE Journal of Oceanic Engineering*, 24(2):237–252, April 1999.

[15] J. C. Simo. A finite strain beam formulation. the three dimensional dynamic problem. part i: formulation and optimal parametrization. *Comp. Meth. Appl. Mech. Eng.*, 72:276–304, 1989.

[16] A. H. Techet and M. S. Triantafyllou. Fluid forces on bodies. Spring term, Ocean Engineering, MIT, 2004.

[17] M. S. Triantafyllou and G. S. Triantafyllou. An efficient swimming machine. *Scientific American*, 272:64–70, March 1995.

[18] M. S. Triantafyllou, G. S. Triantafyllou, and R. Gropalkrishnan. Optimal thrust development in oscillating foils with application to fish propulsion. *J. Fluids Structures*, 7:205–224, 1993.

[19] P. A. Vela, K. A. Morgansen, and J. W. Burdick. Underwater locomotion from oscillatory shape deformations. In *Proceedings of the 41st IEEE Conference on Decision and Control*, pages 2074–2080, Las Vegas, 2002.

[20] J. Yu, L. Wang, and M. Tan. A framework for biomimetic robot fish's design and its realisation. In *American Control Conference*, pages 1593–1598, Portland, 2005.